HAL open science

Past Amazon Basin fluvial systems, insight into the Cenozoic sequences using seismic geomorphology (Marañón Basin, Peru)

Gérôme Calvès, Ysabel Calderon, Vincent Roso, Cédric Bonnel, Martin Roddaz, Stéphane Brusset, Patrice Baby, Peter Clift

To cite this version:

Gérôme Calvès, Ysabel Calderon, Vincent Roso, Cédric Bonnel, Martin Roddaz, et al.. Past Amazon Basin fluvial systems, insight into the Cenozoic sequences using seismic geomorphology (Marañón Basin, Peru). Journal of South American Earth Sciences, 2019, 90, pp.440-452. 10.1016/j.jsames.2018.12.019 . hal-02375767

HAL Id: hal-02375767

https://hal.science/hal-02375767v1

Submitted on 21 Oct 2021

HAL is a multi-disciplinary open access archive for the deposit and dissemination of scientific research documents, whether they are published or not. The documents may come from teaching and research institutions in France or abroad, or from public or private research centers.

L'archive ouverte pluridisciplinaire **HAL**, est destinée au dépôt et à la diffusion de documents scientifiques de niveau recherche, publiés ou non, émanant des établissements d'enseignement et de recherche français ou étrangers, des laboratoires publics ou privés.

Distributed under a Creative Commons Attribution - NonCommercial 4.0 International License

Version of Record: https://www.sciencedirect.com/science/article/pii/S0895981117305242
Manuscript_5435a169d51729cf93f59a5b2659046f

Past Amazon Basin fluvial systems, insight into the Cenozoic sequences using seismic geomorphology (Marañón Basin, Peru).

Authors: Gérôme Calvès[1,*], Ysabel Calderon[1,2]; Vincent Roso[3]; Cédric Bonnel[3]; Martin Roddaz[1,4]; Stéphane Brusset[1], Patrice Baby[4], Peter D. Clift[5]

1. Université Toulouse 3, GET-OMP, 14 Avenue Edouard Belin, 31400, Toulouse, France. [*]Corresponding author: gerome.calves@get.omp.eu

2. PeruPetro, Lima, Peru

3. LFC-R, Université de Pau et des Pays de l'Adour, Avenue de l'Université, 64013, Pau, France.

4. IRD, GET-OMP, 14 Avenue Edouard Belin, 31400, Toulouse, France

5. Louisiana State University (LSU), Baton Rouge, Louisiana 70803, USA

Graphical Abstract:

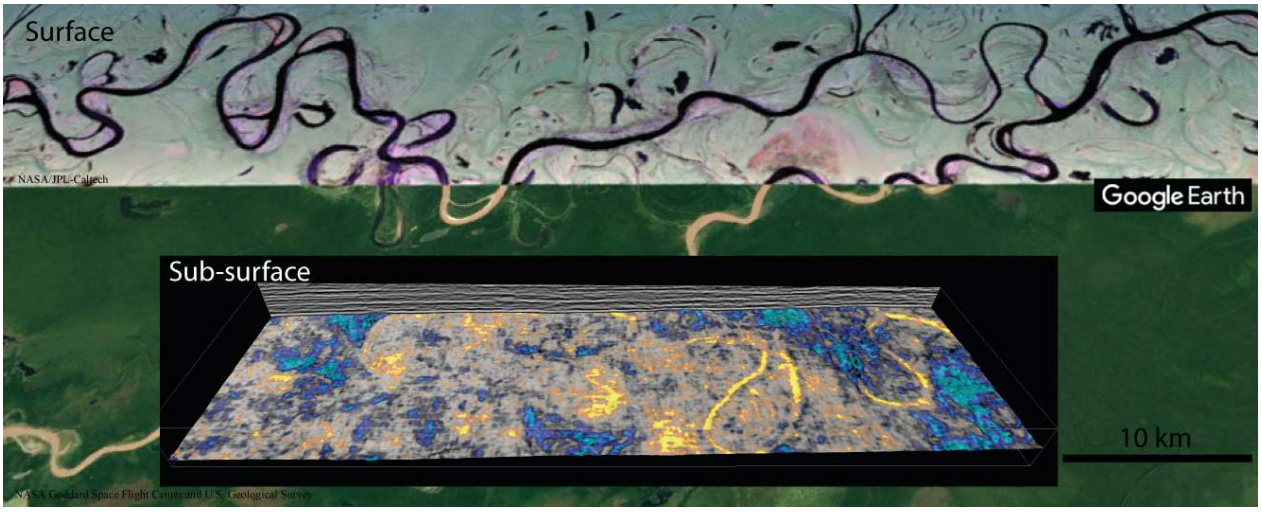

Highlights:

- 3D seismic characterization of buried fluvial systems in the Marañón Basin of Peru
- Evidence of ancient "big rivers" scaled to the modern Amazon Basin fluvial system
- Implications for evolution of sediment load and erosion history of the Andes

© 2018 published by Elsevier. This manuscript is made available under the CC BY NC user license
https://creativecommons.org/licenses/by-nc/4.0/

ABSTRACT (253 words)

This study of the seismic geomorphology of riverine deposits describes and discusses the spatial resolution at which we can detect fluvial features and how the subsequently collected data can help with our understanding of ancient fluvial reservoirs. For this assessment we use three dimensional seismic reflection data, borehole data from ancient deposits in the Marañón foredeep basin of Peru, as well as digital elevation and satellite imagery data from the present day fluvial systems of the Amazonian Basin in the same area of Peru. Based on seismic stratigraphic principles on amplitude display we test parameters to highlight the details of the internal structure of horizons interpreted on continuous wavelets. Seismic attributes such as amplitude, phase, sweetness and spectral decomposition techniques have been successfully applied to make a framework of seismic stratigraphic surfaces that highlight the internal architecture and morphologic details of the studied intervals. This work confirms the presence of a Cenozoic fluvial system in Peru with straight, meandering and anastomosing channels. The observed fluvial features are associated with narrow to medium sized channels (10-~700 m). Evolution of parameters such as sinuosity allows the variation of load in the identified channel features to be constrained. Cenozoic Marañón Basin rivers/streams size and shape are comparable to those observed in the present-day fluvial Amazon Basin. The fluvial dynamics in the study area are identified to be at least present since the deposition of the Pozo-Chambira Formation (Eocene-Oligocene) in the Marañón Basin.

Keywords: Seismic geomorphology, fluvial systems, meanders, channels sinuosity, Amazon Basin, Cenozoic.

1. INTRODUCTION

Paleogeomorphology and drainage organization of fluvial settings has long been of great interest for resource/energy, life habitat, earth cycle research (e.g. Martin, 1966; Southwood, 1977; Fisher et al., 2007) due to the architectural complexity of these types of natural reservoirs and environments. Observations from present-day earth surface fluvial systems are commonly used to inform subsurface interpretation of fluvial-system seismic geomorphology (Posamentier, 2003). Limited publications document ancient river deposits in the subsurface, most of which were deposited in marine-to-fluvial or lacustrine-to-fluvial transition zone settings (e.g.: Weber, 1992; Hardage and Remington, 1999; Posamentier, 2001; Miall, 2002; Sarzalejo and Hart, 2006; Ethridge and Schumm, 2007; Wood 2007; Zeng , 2007; Maynard et al., 2010; Reijenstein et al., 2011; Hubbard et al., 2011; Wang et al., 2012; Qi'an et al., 2015; Zhuo et al., 2015; El-Mowafy and Marfurt, 2016; Alqahtani et al., 2017).

Despite this effort to address some of the most studied objects in the rock record, rivers and their deposits continue to be problematic to earth scientists (Miall, 2014). "Big rivers" are the main arteries that deliver the water and sediment from both orogenic and non-orogenic areas of continents to the world's oceans (Potter, 1978; Miall, 2006; Ashworth and Lewin, 2012; Lewin and Ashworth, 2014). Reconstructing big rivers from ancient deposits is especially challenging due to difficulties in measuring/identifying (and scaling) the architectural elements composing past big rivers. Such deposits are often beyond the scale of conventional outcrops. However, 3D seismic offers the spatial extent to capture the full scale of these elements (Bridge and Tye, 2000) and enables characterization of many ancient rivers whose scale may rival the 'big rivers' of the modern world, such as the Amazon River.

The Amazon River (Figure 1A) ranks number one in terms of global mass transfer from the continents to the oceans (Figure 1B). Indeed, the Amazon River supplies about 20% of the water (Callède et al., 2004), ~10% of the dissolved load (Gaillardet et al., 1997) and ~3% of the suspended load (Milliman and Syvitski, 1992) to the world's oceans. These numbers for transport are only surpassed by the sediment yield in the rivers of south and south-east Asia such as the Huanghe or the Ganges-Brahmaputra (Figure 1B). The present day Amazon Basin is covered by dense tropical vegetation partly protected by nature reserves and is drained by major rivers (Figure 1C). The detailed architecture of the river and its floodplain can be revealed by modern airborne data acquisition, such as Uninhabited Aerial Vehicle Synthetic Aperture Radar (UAVSAR) (Figure 1C). Satellite imagery allows clear discrimination of the two primary elements of this system: the river loaded by suspended fine sediments and the lateral floodplain covered by vegetation.

Recent studies of the outer continental shelf and uppermost Amazon deep-sea fan sediments suggest that the Amazon River initiated as a transcontinental river between 11.8 and 8.7 Ma (Figueiredo et al., 2009; Gorini et al., 2014; Hoorn et al., 2017; van Soelen et al., 2017), and reached its present shape and size during the late Pliocene (Figueiredo et al., 2009). Before the Amazon River transected South America the Middle Miocene environment of the study area was characterized by a long-lived mega-wetland, the Pebas system (Wesselingh et al., 2009; Hoorn et al., 2010). Before the Neogene, the drainage of the Amazon River is postulated to have been to the North with a probable river mouth in the Maracaibo Lake (Roddaz et al., 2010. Hurtado et al., 2018).

The stratigraphy of the Marañón Basin is characterized by two sequences related to the pre-Andean series that consists of Paleozoic–Mesozoic deposits and the Andean series that

corresponds to Cenozoïc marine to continental foreland successions (e.g. Hermoza et al., 2005; Roddaz et al., 2010; Baby et al., 2013; Calvès et al., 2018; Hurtado et al., 2018). Stratigraphic analysis of the continental and fluvial record of the foreland succession (e.g.: Latrubesse et al., 2010) has improved over the past decades with documentation of marine incursion in a globally continental sequence (Westaway, 2006; Wesselingh et al., 2009; Hoorn et al., 2010; Roddaz et al., 2010; Rebata et al., 2016; Jallamillo et al., 2017). In contrast, the structural control on sedimentation and river location in this context has received limited attention (Dumont et al., 1991; Räsänen et al., 1992; Roddaz et al., 2010; Gross et al., 2011; Kröhling, 2017).

The objective of our study is to document the detailed structure of the paleo-fluvial Amazonian system using 3D seismic geomorphology techniques and compare these images to the present day surface drainage geometry of the Amazon Basin in order to discuss the evolution and the preservation of large-scale river deposits in continental drainage areas.

2. MATERIALS AND METHODS

To document the evolution of the present day and paleo-landscape of the Marañón Basin in the Amazon drainage, we have used two data sets. The main data set is 3D multi-channel, post-stack, time-migrated reflection seismic. These data have been acquired over the past decades over oil and gas fields in the Marañón Basin in Peru (Figure 2). The seismic data displayed in this study are zero phase, and follow the Society of Exploration Geophysicist normal polarity, i.e. black peaks indicating an increase in acoustic impedance. The areal extent of the 3D cube is from 90 km^2 to 190 km^2. The 3D grid is subdivided into in-line and cross-line directions, spaced at 30 m. The sampling rate is 4 ms two-way travel time (TWT). In the shallow subsurface the frequency range is 10-70 Hz, with a dominant frequency in the 20-50 Hz range.

Borehole information has been used to constrain the stratigraphy over this area in conjunction with standard seismic stratigraphic principles. The seismic data have been interpreted using various techniques (horizon picking, stratal slicing) and various seismic attributes (Taner and Sheriff, 1977; Taner et al., 1979; Taner, 2003) such as amplitude, phase, sweetness (Hart, 2008) or thin-bed indicators have been extracted and used to enhance interpretation (Figure 3). To screen the data and allow the reader to scroll through the volume, we have extracted seismic amplitude on stratal horizons, and compiled them to produce an animated movie (supplementary data; movie: Hor_slice_Amp.mpg and metadata). A seismic facies chart has been established based on the geometries and acoustic properties observed and quantified on vertical sections and horizontal displays within the 3D volumes. The seismic facies (SF) identified are summarized in Figure 4.

We interpret the morphologic elements found in the 3D data and compare these to morphologies observed in present day river systems (Posamentier, 2000). To accomplish the later, we utilized our second primary data set, satellite images and digital elevation models (DEMs) from the present day surface of the Amazonian Basin. We have used public satellite images and airborne radar (https://uavsar.jpl.nasa.gov), as well as digital elevation models from the NASA Shuttle Radar Topography Mission (SRTM) (https://www2.jpl.nasa.gov/srtm/).

Geomorphological features such as channels (Figure 5) have been quantified following the scheme developed by previous workers on quantitative seismic geomorphology of fluvial features (e.g. Miall 2002; Wood, 2007; Ethridge and Schumm, 2007). Measurements are summarized in Table 1. Parameters of alluvial channels and classification are sourced from Schumm (1985). Paleocurrent flow direction of the fluvial features (trunk rivers, channel, and meander) has been determined following the methods of Miall (2000).

3. RESULTS

3.1. Seismic stratigraphy of the Marañón Basin

The Marañón Basin is a foredeep depozone of the Northern Amazonian foreland basin located between the Andes to the West and the Brazilian and Guyanan shields on its eastern flank (Figure 2). Part of its eastern side is constituted by the Iquitos forebulge (Roddaz et al., 2005) (Figure 2A). We have focused our study on the Cenozoic infill of this basin (Figure 2B), which comprises a thick pile (>3500 m) of clastic sedimentary rocks sourced from the Andes and the South American Cratons. Above the Casablanca-Yahuarango Formation (Cretaceous to lower Paleogene, Figure 2C), the overlying Pozo Shale and Pozo Sandstone (Hermoza et al., 2005) marks the initiation of an overall aggrading fluvial sequence (Chambira, Pebas, Marañón and Corrientes Formations). The seismic images associated to this sequence are characterized by regional >100 km continuous to discontinuous reflections (Figure 2B). At the field scale (less than 10 km), these stratal amplitudes show slight vertical discontinuities (<10–20 ms TWT). These are marked by bright amplitude and high sweetness compared to background values (Figures 3A and 3B). These discontinuous reflections are marked on their edge by phase changes (Figure 3C) and tuning effects marked by the thin-bed detector attribute (Figure 3D).

Below we describe the observations made based on calibrated 3D seismic reflection images. We further interpret these observations in the context of the morphologies that characterize the sedimentary section and summarize its evolution during the Cenozoic.

3.2. Seismic geomorphology of the Paleo-Amazon drainage system

The main seismic facies observed in the studied interval are summarized in Figure 4. Features observed in vertical seismic section are associated with their plan view observed on horizon

amplitude extraction. Discrimination of facies in this fluvial environment cannot be solved only on 2D vertical seismic display. The conformable and parallel seismic reflection makes the plan view and amplitude information essential in recognizing sedimentary features interpreted as channel and streams. Eight SFs have been identified (Figure 4). Seismic facies SF1 to SF5 are interpreted to represent fluvial meandering features, each with various degrees of sinuosity and channel widths that flowed without cross-cutting relationship, whereas seismic facies SF6 is interpreted to reflect deposits from similar types of channels but exhibiting crosscutting relationships. Seismic facies SF7 is interpreted to represent an anastomosing fluvial network. Seismic facies SF1-SF7 occur within a background facies of channel-free material, that is herein interpreted as floodplain overbank sediment (SF8). The peak frequency of these seismic facies ranges from 15 to 45 Hz. The velocity range of the section based on sonic measurement is ~1850 m/s in the shallower section and up to 3800 m/s in the deepest part of the investigated section (over 2.5 sTWT). These velocity values enable bed thickness to be estimated (1/4 wavelength; e.g. Sheriff, 1992) at ~40 m for the higher frequency in the upper section and ~250 m for the lower frequency in lower section. Channels and related parameters have been quantified in plan view following the parameters defined in Figure 5. Channel-widths range from 40 to >650 m (Figure 4). The larger channels show sedimentological features interpreted as channel bars, meander cut-offs and lateral migration of meanders of various sinuosities. The channels can be ranked in three categories based upon their width, following the classification of Gibling (2006). This is as follows: narrow to medium 10s of meters width for individual channels, >100 m wide medium scale composite channels, and >1000 m – wide fluvial systems. Seismic geomorphologic analysis of eight sequential decomposition RGB blended stratal horizon slices provides a temporal history from youngest to oldest stratigraphic levels (Figure 3A; Horizons 8 through 1) and as shown in Figure 6. The seismic facies are interpreted with three main types of fine grained

sediment (mostly shale and silt) associated with splay and other flood plains sediments, as well as two coarse grained lithologies (mostly sand to gravels) associated with channel fills and channel belts.

The oldest horizon within the Marañón Formation, Horizon 8 (pink, Figures 3A and 6A), displays a main channel running in a WNW-ESE trend that is connected to narrow, sparsely-spaced linear to low sinuosity streams. The underlying horizon, Horizon 7, is interpreted to be the Pebas Formation and shows a denser network of parallel medium-to-wide channels associated with rare meandering narrow channels (red, Figure 6B). Horizon 6 shows the transition from Pebas to Chambira Formations and is marked by the interconnection of medium-to-wide channels with N-S to W-E orientations (orange, Figure 6C). Horizon 5, the top of the Chambira Formation (yellow, Figure 6D) shows well developed densely developed interval of high sinuosity, medium width meandering channels. The upper Chambira Formation, Horizon 4 (light green, Figure 6E) shows a greater frequency of wide channels without any characteristic orientation. The channels in this interval show intricate meandering architecture. The transition from upper to lower Chambira Formation at Horizon 3 shows sinuous channels with a potentially anastomosing organization (deep green, Figure 6F). The next underlying interval shown on Horizon 2 is interpreted as the lower Chambira Formation, and shows isolated NNE-SSW oriented, wide meandering belts with high sinuosity meander scars (light blue, Figure 6G). Finally, the oldest Horizon 1, is representative of the Pozo Formation that is characterized by a set of sinuous parallel W-E channels with narrow to medium in width (marine blue, Figure 6H).

3.3. Quantification of channels and fluvial features properties

Quantification of the channel width (n = 420) from the studied seismic horizons interpreted from the Pozo to the Marañón Formations allows a frequency analysis to be conducted and illustrated

by the histogram (Figure 7). The median channel width is 121 m (σ = 107 m). Minimum channel width is 29 m and the maximum value is 641 m (Figure 7A). Based on fluvial channel classifications (Gibling, 2006) 36% of the measured population is classified as being narrow channel. The others are associated to the medium channel group, that have at least of 100 m width. No individual channel features measured in the study area are wider than 641 m. The median channel belt widith (n = 83) is 3598 m (σ = 1295 m), with a minimum measured width of 994 m and a maximum of 7187 m (Figure 7B).

The sinuosity of meandering channels has been quantified (n = 84; Figures 5 and 8) on plan view. The median sinuosity is 1.4 (σ = 0.47) with a minimum value of 1 and a maximum value of 2.9. About 40% of the measured channels have a sinuosity lower than 1.4. Based on the classification scheme of Schumm (1985) for channel sinuosity and load, the measured channels can be divided as follows: with bedload (29.8%) and a sinuosity lower than 1.3, related to a mixed load (53.6%) and a sinuosity higher than 1.3 but and lower than 2, and to suspended load (16.7%) with a sinuosity higher than 2 (Figure 8).

3.4. Temporal evolution and dynamics of Paleo-Amazon drainage system

The Cenozoic evolution of the fluvial architecture of the basin fill is summarized through three parameters (channel width, channel belt width and sinuosity) and measurements of paleocurrent directions (Figure 9). Channel width evolves up-sectionwith apparent increasing size from the Pozo Formation (horizon H1, Figure 9A) to the Chambira Formation (Horizon H2, Figure 9A). Within the Chambira Formation, the upper member shows an increase in channel width with peaks up to 400 m between Horizons H3 and H4, and up to >600 m width between horizons H4 and H6 (Figure 9A). The upper units of the Chambira Formation show a decrease in channel

width that increase again slightly in the upper part of the section, between the Pebas and Marañón Formations (horizons H6 to H8; Figure 9A). The channel belt width increases in association with the type of facies and fluvial patterns, especially with the occurrence of high sinuosity streams (Figures 9B and C). The channel belt width is narrow (~2 km) in the Pozo Formation (H1) while it increase during the emplacement of the Chambira Formation (up to 7.2 km). Then, it decreases in the upper part of the Chambira Formation (horizons H5-H6) and in the Pebas Formation (H7), and finally increase slightly in the Marañón Formation (above H8, Figure 9B). This evolution is highlighted by the sinuosity parameter (Figure 9C). In the same area, the observed modern sinuosity is around 2 where there is the transition from mixed to bed load types (Schumm, 1985). The Pozo Formation fluvial deposits are characterized by sinuosity over 2 and is associated with suspended load transport (horizon H1; Figure 9C). The sinuosity of the Chambira Formation shows a lower member (horizons H2 to H4; Figure 9C) with values associated with low to moderate values (bed load and mixed load) and occasional high values (suspended load). The Upper Member of the Chambira Formation (horizons H5 to H6; Figure 9C) shows low values of sinuosity (mainly bed load). The Pebas and Marañón Formations (horizons H7 to H8; Figure 9C) show mainly low values with some rare high values of sinuosity. The evolution of paleocurrents follows a two steps evolution with NE and SE flowing streams during sedimentation of the Pozo Formation. A wide, south-directed flow was observed during deposition of the Chambira Formation, while a more SE-ward direction of flow was noted for the Pebas and Marañón Formations (Figure 9D). This sequence of aggrading stacked streams and rivers contains three main fluvial features, including: straight, meandering and anastomosing channels (Figure 4 and supplementary data; movie: Hor_slice_Amp.mpg and metadata).

3.5. Present day proximal Amazon drainage and rivers

The present day surface of the Amazon Basin is characterized by a W to E oriented drainage (Figure 1A) with rivers that are both controlled by and incising into topographical structures (Figure 10A) related to the recent evolution of the South American Plate and the Andean mountain range (e.g.: Räsänen et al., 1987, 1990, 1992; Roddaz et al., 2005; Shephard et al., 2010; Latrubesse, 2015; Stokes et al., 2018). The Marañón Basin sits at the confluence of two main river networks, one originating from the Napo-Pastaza Fan to the northwest (Figure 10A; Bernal, et al., 2011) and a second from the Fitzcarrald Arch to the southwest (Espurt et al., 2007). These two drainages combine at the town of Iquitos to form the Rio Solimões that run to the Amazon River mouth and from there into the Atlantic Ocean. An SRTM digital elevation model has been extracted to document the shape and size of the rivers and drainage from the Andes to Iquitos (Figure 10B to 10E). The NW-SE present river located above the seismic cube is the Rio Pataza (Figure 6 and supplementary data movie). We have seen that since the Cenozoic the river network and types evolved in two major steps recorded by the Pozo, Chambira, Pebas and Marañón Formations. Downstream the rivers are able to incise the edge of the older watershed, related with the recent rise of the Iquitos Arch along a NW-SE axis (Figure 10C). An incision is presently filled by highly sinuous meanders and streams that are controlled by kilometer wide lows (Figure 10C). Laterally the Pastaza-Corrientes transition band (Figure 10A) with its low land and flood plains shows rivers that are isolated with more linear streams and lower sinuosity (Figure 10D). Finally, after the connection of the Rio Tigre, Marañón and Ucayali, a wide to very large river flows to the NE with large point bar and cut off (Figure 10E). All these present day settings represent the large diversity of rivers and streams along this proximal part of the Amazon Basin.

4. DISCUSSION

4.1. Comparing present day and past morphologies of rivers using different images sources

We have documented the seismic geomorphology of the sedimentary infill of part of the Marañón Basin and the present day fluvial network of the western Amazon Basin. The areal cover and vertical penetration of the subsurface data allows channels associated to a paleo-river network to be recognized. Characterization of the vertical resolution of a channel in subsurface imaging is a difficult task, whereas the lateral extend is easier to achieve. In contrast, measurements of lateral extent based on downhole wireline logs is challenging (Bridge and Tye, 2000) but thickness is easy to quantify (e.g.; Gibling, 2006). Here we discuss the sizes, shape recognition and potential risk when using analogues and various sources of data displayed in plan view analysis, i.e. the comparison of relative resolution (Figure 11). From a high resolution UAVSAR image, a Landsat image or a stratal seismic horizon we can try to understand the predictive nature of the observations. From a giant meander in the Rio Ucayali, a reference 5x5 km box allows a river and its internal structures such as meanders, bars, oxbow lakes or a portion of them to be framed regardless of where the box is located (Figure 11A). Using a set of Landsat images (Figure 11B), we can characterize the shape of various rivers even for the widest meanders, oxbow lakes and bars. However, the lateral continuity of the channel laterally cannot be described. In contrast, the 3D images of the channels derived from the seismic reflection data allow a mixed perspective with a lower resolution (Figure 11C). A 5x5 km box applied to a given 3D stratal horizon allows the definition of the channel and its content, especially when using spectral decomposition and color blend display (Partyka et al., 1999). Targeting channels and their net infill is the goal of natural resources exploration if such work is to define good quality reservoirs. Comparison of the ancient geologic reservoir and its present day analogues can help to assist with reservoir properties prediction (Alexander, 1993; Clift et al., 2018). The fluvial sedimentary environment

is a challenge because the shape of a river can be associated with various locations on the erosional-depositional profile and upstream controls (Schumm, 2005).

4.2. Persistent fluvial landscape

The fluvial features described above characterize most of the Cenozoic infill of the Marañón Basin and the present day surface of the Amazon Basin. Our study outlines the preservation of fluvial geomorphic elements in the rock record, as observed in modern sedimentary basins (Weissman et al., 2015). The difficulty in establishing long-term quantified rates of sedimentation and related supply from mountain ranges could be solved using the fluvial features observed in the subsurface. The morphology of the present day Amazon Basin and its meandering rivers and floodplain are driven by the sediment supply (Constantine et al., 2014). Thus, investigation of calibrated fluvial features could allow the paleo-sediment supply of the Cenozoic Andes to the Amazon Basin to be quantified.

The role of deep solid-earth structure on the vertical movements of the Earth's surface and the processes related to drainage/fluvial dynamics at continental scale has been investigated (e.g., Flament et al., 2015; Rodríguez Tribaldos et al., 2017). Limitation of the models mean that the earlier history of the Amazon Basin cannot be solved in this way. The Late Eocene to Early Oligocene times are predicted to represent periods of low incision rates over the entire Amazon catchment (Rodríguez Tribaldos et al., 2017). Incision rates increased in the Early Miocene in those areas west of the Guyana and Brazilian Cratons. The incision rate near the Cordillera only increased at 11 Ma. Our observations of the early dynamics of incision and deposition of fluvial system in the proximal part of the Amazon Basin near the Cordillera are in agreement with this

timing of uplift. Fluvial systems of continental drainage have existed since the transition from the Pozo to the Chambira Formations, i.e., at least since the Oligocene.

5. CONCLUSIONS

Modern techniques of seismic imaging and geomorphology have allowed the sedimentological evolution of the Marañón Basin in Peru to be reconstructed. We document the fluvial history of the Amazon Basin at the scale of the Cenozoic for the first time. This sequence of an aggradational stack of streams and rivers contains three main fluvial features, including straight, meandering and anastomosing channels. The size and shape of the channels observed are comparable with present day observations from DEMs or satellite images of Amazon Basin drainage and its river network. This study represents a first step toward a methodology for regional exploration of the fluvial record through the use of modern seismic geomorphology techniques in the Amazon Basin. Yet far from answering all the points raised by other studies of fluvial geomorphology, further detailed mapping of the Cenozoic sedimentary basins of the Amazon Basin is needed (e.g. Solimões, Amazonas). These work must stretch from the source to the sink if it is to depict the sediment routing systems (Allen, 2017), from the foothills of the Andes Mountains to the Amazon mouth and its slope margin deep-water fan. Specific aspects that need to be developed and tested included: (1) integration of borehole resistivity imagery to constrain paleoflow of stream and rivers, (2) quantitative geomorphology and stream flow orientation, (3) combining tracer techniques of sediments to define the sources of sediments. Update of the paleogeographic map for this specific period of geological time will allow better constraints on the evolution of the South American plate that is relatively inaccessible to field

study compared to other continents. Acquisition of vertical 'transitional' subsurface data ranging from the surface to the youngest resolved seismic reflection image in subsurface could allow a full and continuous analysis of the evolution of this giant sedimentary basin.

ACKNOWLEDGEMENTS

GC would like to thank PeruPetro for allowing this work being published. Financial support from Institut-Carnot IsiFor (Agence National de la Recherche) is appreciated. Thanks to IHS-Kingdom, dGB Earth Sciences OpendTect and GeoTeric, for their academic software donations and support. Palaeocurrent diagram were produced using freeware Rose 2.1.0 (Todd Thompson Software). Many thanks to A. Hartley (University of Aberdeen) and S. Leleu (ENSEGID - IPBordeaux) for earlier discussion and perspectives on fluvial sedimentary systems. Thanks to C. Série (ConocoPhillips) and C. Kirkham (University of Oxford) for help during the manuscript revision. An earlier reviewed version of this work has benefited from valuables review performed by L. Wood (Colorado School of Mines), Y. Sun (Chevron), and J. Bhattacharya (University of Houston). Tiago Alves (Cardiff University), an anonymous reviewer, the managing editor Kerry McCarney-Castle and the regional editor Victor Ramos, are thanked for their support and constructive comments.

TABLES

Table 1: Channels morphometry from Marañón Basin Cenozoic infill, Peru

Horizon number	Seismic Stratigraphy	Formation name	Depth		Channel Width					Channel length on one wavelength (La)	Meander wavelength
			min	max							
			s (TWT)		(m)					(m)	(m)

1		Maranon	0,479	0,661	200	220	260	140	120	9832	464
2			0,499	0,681	130	141	87	140	145	6058	495
3			0,519	0,701	166	147	162	146	167	9328	360
4			0,557	0,727	113	170	79	120	105	7719	540
5	H8		0,587	0,757	128	162	205	154	213	7760	687
6			0,617	0,787	119	125	116	154	190	5611	320
7			0,659	0,828	188	180	102	148	134	5189	246
8			0,684	0,845	106	160	125	122	125	2620	221
9			0,7	0,864	97	120	113	80	97	7842	706
10			0,72	0,884	144	68	58	74	158	4825	453
11			0,747	0,902	242	305	88	98	65	8355	792
12			0,757	0,9112	123	101	155	74	90	5007	363
13			0,767	0,922	131	94	76	117	44	4279	340
14	H7	Pebas	0,791	0,947	213	118	85	115	51	4306	305
15			0,824	0,984	101	121	112	71	146	6987	627
16			0,843	0,992	73	95	123	46	67	3951	380
17			0,868	1,019	102	68	70	130	68	7747	535
18			0,892	1,048	70	64	84	89	149	9423	426
19			0,902	1,067	76	82	60	91	81	3283	281
20			0,912	1,077	100	117	124	109	156	6696	556
21			0,922	1,087	104	50	42	59	54	3901	312
22			0,94	1,082	65	75	104	88	42	5998	410
23	H6		0,95	1,092	97	96	118	73	159	10205	922
24			0,975	1,117	134	95	127	68	88	5050	408
25			1	1,142	143	71	94	62	46	3227	268
26			1,004	1,17	109	55	74	29	55	1645	147
27			1,024	1,19	106	166	88	96	180	4693	318
28			1,064	1,219	294	223	259	157	293	6877	601
29			1,084	1,239	99	131	86	50	171	3439	305
30			1,104	1,259	421	494	350	343	403	15083	1458
31			1,124	1,279	358	288	249	178	282	6435	426
32			1,144	1,299	527	615	503	301	615	8369	806
33			1,186	1,327	472	118	159	308	74	7783	400
34			1,201	1,355	450	222	401	617	439	11117	1045
35			1,221	1,378	97	329	138	197	162	14302	1194
36	H5		1,241	1,395	200	560	312	169	286	6604	347
37			1,261	1,415	425	149	282	223	235	4427	325
38			1,296	1,442	293	136	302	204	121	6375	455
39			1,316	1,462	215	79	79	260	161	5346	220
40			1,348	1,495	127	94	97	103	145	9842	642
41			1,377	1,519	627	641	594	550	221	20960	1837
42			1,406	1,543	168	357	262	372	437	13962	1203

43			1,424	1,566	142	236	246	279	198	7017	610
44			1,442	1,589	81	98	71	90	64	8471	455
45	H4		1,46	1,613	250	169	55	74	38	5787	459
46			1,47	1,623	166	168	262	70	155	5272	410
47			1,498	1,632	233	333	444	353	404	12693	701
48			1,532	1,661	169	189	188	222	232	9495	466
49			1,549	1,677	113	117	101	50	110	10349	584
50			1,566	1,693	189	249	171	140	306	8724	458
51			1,583	1,712	168	109	87	136	137	6086	351
52	H3		1,6	1,73	134	183	95	123	91	5915	394
53			1,61	1,74	98	156	127	220	109	5158	195
54			1,62	1,75	310	180	151	202	137	5690	287
55			1,633	1,761	85	119	94	220	276	4844	386
56			1,65	1,776	195	99	158	135	278	4849	346
57			1,684	1,807	103	170	125	106	120	4477	388
58			1,7	1,825	127	112	168	67	84	4340	207
59			1,717	1,842	98	47	99	84	75	1996	197
60			1,734	1,86	334	149	145	110	125	6474	450
61			1,765	1,896	139	110	103	68	96	4649	292
62			1,78	1,915	147	90	103	145	161	5792	503
63	H2	Chambira	1,795	1,933	254	149	116	139	105	8456	576
64			1,815	1,953	174	203	190	187	203	12707	684
65			1,832	1,965	200	110	165	140	116	4726	374
66			1,847	1,991	106	227	152	210	183	7382	442
67			1,868	2,011	153	70	83	75	207	3740	284
68			1,888	2,024	113	92	95	96	135	3291	136
69			1,905	2,042	106	114	121	158	125	9318	622
70			1,912	2,067	123	66	81	96	97	5089	273
71			1,947	2,086	146	72	94	93	138	5739	498
72			1,957	2,096	67	114	119	137	148	14184	684
73			1,967	2,106	102	86	73	82	72	4829	339
74			1,977	2,116	165	134	108	139	123	6870	240
75			1,987	2,126	96	74	118	83	104	4915	350
76			1,997	2,136	60	66	77	101	44	2707	193
77			2,019	2,154	41	60	47	41	76	8178	813
78			2,041	2,157	96	49	82	94	51	2266	126
79			2,065	2,178	126	94	77	92	80	1945	175
80			2,071	2,209	123	109	205	101	199	5396	380
81			2,094	2,24	67	86	88	103	79	2727	197
82			2,113	2,256	69	42	60	62	72	4323	148
83	H1	Pozo	2,143	2,28	65	81	98	100	84	1907	72
84			2,158	2,321	128	226	84	127	159	4490	196

85		Present day surface							11917	620
86		Present day surface							43900	2120

FIGURES CAPTIONS

Figure 1: A. Amazon Basin drainage outline over SRTM digital elevation model and HydroSHEDS river network (EO, NASA). B. Major world rivers yield (drainage area >10^3 km²) as a function of drainage area (Syvitski et al., 2005). C. Comparison of two different satellite images over the Rio Ucayali (UAVSAR data courtesy NASA/JPL-Caltech, Landsat imagery courtesy of NASA Goddard Space Flight Center and U.S. Geological Survey), note the resolution over the UAVSAR image that highlights the detailed architecture of the meanders and lateral accretion formed by the Rio Ucayali.

Figure 2: (A) Example of the Marañón Basin Cenozoic infill from the (B) seismic line that illustrates the regional geometry across the Marañón Basin from the foothills of the Andes (SW) to the Iquitos Arch (NE) and (C) detailed lithologic and stratigraphic information from a well located south of the regional cross section. Note the thickness of the Chambira Formation that spans from Eocene to the Upper Oligocene, the aggrading pattern is associated with floodplain and fluvial channel and sand sheets stacking. The Neogene Pebas, Marañón and Corrientes Formations show more variations in lithological content.

Figure 3: (A) Seismic reflection amplitude and stratigraphy of the Marañón Basin Cenozoic infill. (B) The relatively continuous to discontinuous character of the reflection strength is enhanced by the sweetness attribute, thick sands are associated with high sweetness values (i.e. blue or yellow colors). (C and D) The phase and thin-bed attribute are used to highlight the pinch-out and tuning

of the channels and its infill. The colored triangles are selected horizons displayed in Figure 6. Location of the seismic line is located in Figure 2A and in Figure 6.

Figure 4: Quantitative geomorphologic measures along a horizon slice with sweetness attribute display. Channel width (W), meander belt width (MBW), channel length on one wavelength (La), meander wavelength (ML), and radius of curvature (RC). Sinuosity is calculated by channel length divided by meander wavelength.

Figure 5: Seismic facies observed and interpreted in the Marañón Basin within the Cenozoic infill. All seismic sections and plan views of the facies are scaled with the same amplitude values and vertical/horizontal scales.

Figure 6: Evolution of the fluvial patterns observed and interpreted on colored blended spectral decomposition horizons highlighting the main changes in the stratigraphy of the Cenozoic sequence of the Marañón Basin. The RGB compositions show frequency 39, 32, and 29 Hz respectively. The color code for each slice A to H corresponds to the arrows on the seismic section displayed in Figure 3A. The RBG blend horizons are displayed from shallower part to deep part of the basin. The white line drawing is associated to features related to fluvial geometries, main channels and extensive fluvial features are interpreted following facies scheme in Figure 5.

Figure 7: Statistical analysis of quantified fluvial channel width from the Cenozoic record of the Marañón Basin. Channel width classification is from Gibling (2006), narrow to medium channels correspond to 100 m width.

Figure 8: Statistical analysis of sinuosity from quantified meanders of the Cenozoic record of the Marañón Basin. Classification of alluvial channels by sediment load is based on Schumm (1985). The cutoffs used to differentiate the type of channels based on sinuosity are 1.3 and 2.

Figure 9: Stratigraphic evolution of channels width, belt width, sinuosity and paleocurrents from the Cenozoic record of the Marañón Basin. This reconstruction is based on observation, interpretation and quantification of 84 seismic stratigraphic surfaces extracted in the seismic reflection 3D cube.

Figure 10: (A) Present day surface of the western part of the Amazon Basin. Inset of fluvial systems from the proximal Rio Pastaza and the Napo-Pastaza Megafan to intermediate Rio Ucayali south of Iquitos. (B) Example of 3D seismic survey used for this study, note the areal extent of a survey compared to the natural features observed at its edge, the rivers flow from NW to SE. (C) Example of meandering and laterally incising paleodrainage, in relation to the NW-SE plunging Iquitos Arch. (D) Low land and flood plain in the Pastaza-Corrientes transition band north of the Rio Marañón, note the various abandoned splays and the amount of meandering channels. (E) Encased Rio Ucayali meandering channel with large point bar and cut off loops. Note the variety of properties of the various channels and their lateral lowland landscapes. DEM from B to E are at the same horizontal scale, vertical relief is lows for dark and bright for highs. DEM are sourced from SRTM (NASA), UAVSAR data courtesy NASA/JPL-Caltech, *Landsat* imagery *courtesy of* NASA Goddard Space Flight Center and U.S. Geological Survey.

Figure 11: Comparative fluvial views from detailed (A) UAVSAR over the Rio Ucayali, (B) Landsat over rivers and streams from the Amazon Basin and (C) 3D seismic interpreted spectral decomposition images/maps from the Marañón Basin. Note the 5x5 km black square that allows

comparison of architectural elements from the three different sourced images. DEM are sourced from SRTM (NASA), UAVSAR data courtesy NASA/JPL-Caltech, *Landsat* imagery *courtesy of* NASA Goddard Space Flight Center and U.S. Geological Survey. Fluvial features: channel, bars, meanders, lateral accretion, oxbow lake (ox. l).

REFERENCES

Alexander, J. (1993). A discussion on the use of analogues for reservoir geology. Geological Society, London, Special Publications, 69(1), 175–194.

Allen, P. (2017). *Sediment Routing Systems: The Fate of Sediment from Source to Sink*. Cambridge: Cambridge University Press. doi:10.1017/9781316135754

Alqahtani, F. A., Jackson, C. A.-L, Johnson, H.D., Som, M. R. B., 2017. Controls On the Geometry and Evolution of Humid-Tropical Fluvial Systems: Insights From 3D Seismic Geomorphological Analysis of the Malay Basin, Sunda Shelf, Southeast Asia. Journal of Sedimentary Research, 87 (1), 17–40.

Ashworth, P. J., Lewin, J., 2012. How do big rivers come to be different? Earth-Science Reviews, 114(1–2), 84–107.

Baby, P., M. Rivadeneira, R. Barragán, F. Christophoul, 2013. Thick-skinned tectonics in the Oriente foreland basin of Ecuador, In: Nemčok M., Mora A. R., Cosgrove J. W. (eds) Thick-Skin-Dominated Orogens: From Initial Inversion to Full Accretion, Geological Society, London, Special Publications, 377, 59–76.

Bernal, C., Christophoul, F., Darrozes, J., Soula, J.-C., Baby, P., & Burgos, J. (2011). Late Glacial and Holocene avulsions of the Rio Pastaza Megafan (Ecuador--Peru): frequency and controlling factors. *International Journal of Earth Sciences*, *100*(7), 1759–1782. https://doi.org/10.1007/s00531-010-0555-9

Bridge, J. S., Tye, R. S., 2000. Interpreting the Dimensions of Ancient Fluvial Channel Bars, Channels, and Channel Belts from Wireline-Logs and Cores. AAPG Bulletin, 84(8), 1205–1228.

Callède, J., Guyot, J. L., Ronchail, J., L'Hôte, Y., Niel, H., de Oliveira, E., 2004. Evolution du débit de l'Amazone à Óbidos de 1903 à 1999/Evolution of the River Amazon's discharge at Óbidos from 1903 to 1999. Hydrological Sciences Journal, 49, 85–97.

Calvès, G., Calderón, Y., Enriquez, C. H., Brusset, S., Santini, W., & Baby, P. (2018). Mass balance of cenozoic andes-amazon source to sink system—marañón basin, Peru. Geosciences (Switzerland), 8(5). https://doi.org/10.3390/geosciences8050167

Clift, P.D., Olson, E.D., Lechnowskyj, A., Moran, M.G., Barbato, A., & Lorenzo, J.M., (2018). Grain-size Variability within a Mega-scale Point Bar System, False River, Louisiana. Sedimentology. doi:10.1111/sed.12528.

Constantine, J. A., Dunne, T., Ahmed, J., Legleiter, C., & Lazarus, E. D., 2014. Sediment supply as a driver of river meandering and floodplain evolution in the Amazon Basin. Nature Geosci, 7(12), 899–903.

Dumont, J. F., Deza, E., & Garcia, F. (1991). Morphostructural provinces and neotectonics in the Amazonian lowlands of Peru. *Journal of South American Earth Sciences*, *4*(4), 373–381. https://doi.org/https://doi.org/10.1016/0895-9811(91)90008-9

El-Mowafy, H. Z., Marfurt, K. J., 2016. Quantitative seismic geomorphology of the middle Frio fluvial systems, south Texas, United States. AAPG Bulletin, 100(4), 537–564.

Ethridge, F.G., Schumm, S.A., 2007. Fluvial seismic geomorphology: a view from the surface: Geological Society, London, Special Publications, 277, 205–222.

Espurt, N., Baby, P., Brusset, S. Roddaz, M., Hermoza, W., Regard, V., Antoine, P.-O., Salas-Gismondi, R., Bolaños, R., 2007. How does the Nazca Ridge subduction influence the modern Amazonian foreland basin?. Geology, 35, 515–518.

Figueiredo, J., Hoorn, C., Van der Ven, P., Soares, E., 2009. Late Miocene onset of the Amazon River and the Amazon deep-sea fan: Evidence from the Foz do Amazonas Basin. Geology, 37, 619–622.

Fisher, S. G., Heffernan, J. B., Sponseller, R. A., & Welter, J. R. (2007). Functional ecomorphology: Feedbacks between form and function in fluvial landscape ecosystems. *Geomorphology*, *89*(1), 84–96. https://doi.org/https://doi.org/10.1016/j.geomorph.2006.07.013

Flament, N., Gurnis, M., Müller, R. D., Bower, D. J., Husson, L., 2015. Influence of subduction history on South American topography. Earth and Planetary Science Letters, 430(Supplement C), 9–18.

Gaillardet, J., Dupre, B., Allegre, C. J., Négrel, P., 1997. Chemical and physical denudation in the Amazon River Basin. Chemical Geology, 142, 141–173.

Gibling, M. R., 2006. Width and Thickness of Fluvial Channel Bodies and Valley Fills in the Geological Record: A Literature Compilation and Classification. Journal of Sedimentary Research, 76, 731–770.

Gorini, C., Haq, B.U., dos Reis, A.T., Silva, C.G., Cruz, A., Soares, E., Grangeon, D., 2014. Late Neogene sequence stratigraphic evolution of the Foz do Amazonas Basin, Brazil. Terra Nova 26, 179–185.

Gross, M., Piller, W. E., Ramos, M. I., & Douglas da Silva Paz, J. (2011). Late Miocene sedimentary environments in south-western Amazonia (Solim?es Formation; Brazil). *Journal of South American Earth Sciences*, *32*(2), 169–181. https://doi.org/10.1016/j.jsames.2011.05.004

Hardage, B. A., Remington, R. L., 1999. 3-D seismic stratal-surface concepts applied to the interpretation of a fluvial channel system deposited in a high-accomodation environment. Geophysics, 64, 609–620.

Hart, B. S. 2008. Channel detection in 3-D seismic data using sweetness. AAPG Bulletin, 92, 733–742.

Hermoza, W., Brusset, S., Baby, P., Gil, W., Roddaz, M., Guerrero, N., Bolaños, R., 2005. The Huallaga foreland basin evolution: Thrust propagation in a deltaic environment, northern Peruvian Andes. Journal of South American Earth Sciences, 19(1), 21–34.

Hoorn, C., Wesselingh, F. P., Ter Steege, H., Bermudez, M. A., Mora, A., Sevink, J., Antonelli, A., 2010. Amazonia through time: Andean uplift, climate change, landscape evolution, and biodiversity. Science, 330, no.6006, 927–931.

Hoorn, C., Bogotá-A, G.R., Romero-Baez, M., Lammertsma, E.I., Flantua, S.G.A., Dantas, E.L., Dino, R., do Carmo, D.A., Chemale Jr, F., 2017. The Amazon at sea: Onset and stages of the Amazon River from a marine record, with special reference to Neogene plant turnover in the drainage basin. Glob. Planet. Change 153, 51–65.

Hubbard, S. M., Smith, D. G., Nielsen, H., Leckie, D. A., Fustic, M., Spencer, R. J., Bloom, L., 2011. Seismic geomorphology and sedimentology of a tidally influenced river deposit, Lower Cretaceous Athabasca oil sands, Alberta, Canada. AAPG Bulletin, 95, 1123–1145.

Hurtado, C., Roddaz, M., Santos, R. V., Baby, P., Antoine, P.-O., Dantas, E. L., 2018 Cretaceous-early Paleocene drainage shift of Amazonian rivers driven by Equatorial Atlantic Ocean opening and Andean uplift as deduced from the provenance of northern Peruvian sedimentary rocks (Huallaga basin). Gondwana Research 63, 152-168, doi:10.1016/j.gr.2018.05.012.

Jaramillo, C., Romero, I., D'Apolito, C., Bayona, G., Duarte, E., Louwye, S., Escobar, J., Luque, J., Carrillo-Briceño, J. D., Zapata, V., Mora, A., Schouten, S., Zavada, M., Harrington, G., Ortiz, J., Wesselingh, F. P., 2017. Miocene flooding events of western Amazonia. Science Advances, 3(5), doi: 10.1126/sciadv.1601693

Kröhling, D. M., 2017. Analysis of the Quaternary climatic and tectonic forcing along some different tectonic settings of South America. Quaternary International, 438, 1–3.

Latrubesse, E. M., 2015. Large rivers, megafans and other Quaternary avulsive fluvial systems: A potential "who's who" in the geological record. Earth-Science Reviews, 146, 1–30.

Latrubesse, E. M., Cozzuol, M., da Silva-Caminha, S. A. F., Rigsby, C. A., Absy, M. L., Jaramillo, C., 2010. The Late Miocene paleogeography of the Amazon Basin and the evolution of the Amazon River system. Earth-Science Reviews, 99(3), 99–124.

Lewin, J., Ashworth, P. J., 2014. Defining large river channel patterns: Alluvial exchange and plurality. Geomorphology, 215, 83–98.

Martin, R, 1966. Paleogeomorphology and its application to exploration for oil and gas (with examples from western Canada). AAPG Bulletin, 50, 2277–2311.

Maynard, J. R., Feldman, H. R., Alway, R., 2010. From bars to valleys: the sedimentology and seismic geomorphology of fluvial to estuarine incised-valley fills of the Grand Rapids Formation (Lower Cretaceous), Iron River Field, Alberta Canada. Journal of Sedimentary Research, 80, 611–638.

Miall, A. D., 2000. Basin-Mapping Methods. In: Principles of Sedimentary Basin Analysis. Springer, Berlin, Heidelberg

Miall, A. D., 2002. Architecture and sequence stratigraphy of Pleistocene fluvial systems in the Malay Basin, based on seismic time-slice analysis. AAPG Bulletin, 86, no.7, 1201–1216.

Miall, A. D., 2006. How do we identify big rivers? And how big is big?. Sedimentary Geology, 186, 39–50.

Miall, A. D., 2014. Fluvial Depositional Systems, Springer, 316 p.

Milliman, J. D., Syvitski, J. P., 1992. Geomorphic/tectonic control of sediment discharge to the ocean: the importance of small mountainous rivers. The Journal of Geology, 100, 525–544.

Partyka, G., Gridley, J., Lopez, J., 1999. Interpretational applications of spectral decomposition in reservoir characterization. The Leading Edge, 18, 353–360.

Posamentier, H. W., 2000. Seismic stratigraphy into the next millennium; a focus on 3D seismic data: AAPG Annual Conference, New Orleans, LA, 16-19 April, 2000, A118.

Posamentier, H. W., 2001. Lowstand alluvial bypass systems: incised vs. unincised. AAPG Bulletin, 85, 1771–1793.

Posamentier, H. W., 2003. Depositional elements associated with a basin floor channel-levee system: case study from the Gulf of Mexico. Marine and Petroleum Geology, 20, 677–690.

Potter, P. E., 1978. Significance and Origin of Big Rivers. The Journal of Geology, 86(1), 13–33.

Qi'an, M., Shun, Z., Guoxin, S., Xiuli, F., Chao, W., Yao, S., 2015. A seismic geomorphology study of the fluvial and lacustrine-delta facies of the Cretaceous Quantou-Nenjiang Formations in Songliao Basin, China. Marine and Petroleum Geology, 78, 836–847.

Räsänen, M. E., Salo, J. S., Kalliola, R. J., 1987. Fluvial Perturbance in the Western Amazon Basin: Regulation by Long-Term Sub-Andean Tectonics. Science, 238(4832), 1398–1401.

Räsänen, M. E., Salo, J. S., Jungnert, H., Pittman, L. R., 1990. Evolution of the Western Amazon Lowland Relief: impact of Andean foreland dynamics. Terra Nova, 2(4), 320–332.

Räsänen, M., Neller, R., Salo, J., Jungner, H., 1992. Recent and ancient fluvial deposition systems in the Amazonian foreland basin, Peru. Geological Magazine, 129(3), 293–306.

Rebata H., L. A., R?s?nen, M. E., Gingras, M. K., Vieira, V., Barberi, M., & Irion, G. (2006). Sedimentology and ichnology of tide-influenced Late Miocene successions in western Amazonia: The gradational transition between the Pebas and Nauta formations. *Journal of South American Earth Sciences*, *21*(1–2), 96–119. https://doi.org/10.1016/j.jsames.2005.07.011

Reijenstein, H. M., Posamentier, H. W., Bhattacharya, J. P., 2011. Seismic geomorphology and high-resolution seismic stratigraphy of inner-shelf fluvial, estuarine, deltaic, and marine sequences, Gulf of Thailand. AAPG Bulletin, 95, 1959–1990.

Roddaz, M., Baby, P., Brusset, S., Hermoza, W., Darrozes, J. M., 2005. Forebulge dynamics and environmental control in Western Amazonia. The case study of the Arch of Iquitos (Peru): Tectonophysics, 399, 87–108.

Roddaz, M., Hermoza, W., Mora, A., Baby, P., Parra, M., Christophoul, F., Brusset, S., Espurt, N., 2010. Cenozoic Sedimentary Evolution of the Amazonian Foreland Basin System, in: Hoorn, C., Wesselingh, F.P. (Eds.), Amazonia: Landscape and Species Evolution. Wiley-Blackwell Publishing Ltd., pp. 61–88

Rodríguez Tribaldos, V., White, N. J., Roberts, G. G., Hoggard, M. J., 2017. Spatial and temporal uplift history of South America from calibrated drainage analysis. Geochem. Geophys. Geosyst., 18, doi:10.1002/2017GC006909.

Sarzalejo, S., Hart, B. S., 2006. Stratigraphy and lithologic heterogeneity in the Mannville Group (southeast Saskatchewan) defined by integrating 3-D seismic and log data. Bulletin of canadian petroleum geology, 54, 138–151.

Schumm, S. A., 1985. Patterns of Alluvial Rivers. Annual Review of Earth and Planetary Sciences, 13(1), 5–27.

Schumm, S. A., 2005. River Variability and Complexity. Cambridge University Press, Cambridge.

Shephard, G. E., Müller, R. D., Liu, L., Gurnis, M., 2010. Miocene drainage reversal of the Amazon River driven by plate–mantle interaction. Nature Geoscience, 3, 870–875.

Sheriff, R. E., 1992. Vertical and Lateral Seismic Resolution and Attenuation: Part 7. Geophysical Methods. In D. Morton-Thompson and A. M. Woods, eds., Development Geology Reference Manual, AAPG Methods in Exploration Series, 10, 388–389.

Southwood, T.R.E., 1977. Habitat, the templet for ecological strategies. Journal of Animal Ecology 46, 337–365.

Stokes, M. F., Goldberg, S. L., & Perron, J. T. (2018). Ongoing River Capture in the Amazon. *Geophysical Research Letters*, *45*(11), 5545–5552. https://doi.org/10.1029/2018GL078129

Syvitski, J.P.M., Kettner, A.J., Correggiari, A., Nelson, B.W., 2005. Distributary channels and their impact on sediment dispersal. Marine Geology, 222–223, 75–94.

Taner, M. T., Sheriff, R. E., 1977. Application of amplitude, frequency, and other attributes to stratigraphic and hydrocarbon determination: In: AAPG Memoir 26: Seismic Stratigraphy-Applications to Hydrocarbon Exploration (Ed. C.E. Payton), 301–327.

Taner, M., Koehler, F., Sheriff, R., 1979. Complex seismic trace analysis. Geophysics, 44(6), 1041–1063.

Taner, M.T., 2003. Attributes revisited. http://www.rocksolidimages.com/attributes-revisited

van Soelen, E.E., Kim, J.-H., Santos, R.V., Dantas, E.L., Vasconcelos de Almeida, F., Pires, J.P., Roddaz, M., Sinninghe Damsté, J.S., 2017. A 30 Ma history of the Amazon River inferred from terrigenous sediments and organic matter on the Ceará Rise. Earth Planet. Sci. Lett. 474, 40–48.

Wang, Z., Yin, C., Fan, T., X., Lei, 2012. Seismic geomorphology of a channel reservoir in lower Minghuazhen Formation, Laizhouwan subbasin, China. Geophysics, 77, 187–195.

Weber, K. J., 1992. The Use of 3-D Seismic in Reservoir Geological Modelling. In: The Geological Modelling of Hydrocarbon Reservoirs and Outcrop Analogues. Blackwell Publishing Ltd. 181–188.

Weissmann, G. S., Hartley, A. J., Scuderi, L. A., Nichols, G. J., Owen, A., Wright, S., Felicia, A. L., Holland, F., Anaya, F. M. L. , 2015. Fluvial geomorphic elements in modern sedimentary basins and their potential preservation in the rock record: A review. Geomorphology, 250, 187–219.

Wesselingh, F. P., Hoorn, C., Kroonenberg, S. B., Antonelli, A., Lundberg, J. G., Vonhof, H. B., Hooghiemstra, H., 2009. On the origin of Amazonian landscapes and biodiversity: a synthesis. In C. Hoorn and F. P. Wesselingh, eds, Amazonia: Landscape and Species Evolution: A look into the past, Wiley-Blackwell Publishing Ltd., Oxford, UK. 419–431.

Westaway, R., 2006. Late Cenozoic sedimentary sequences in Acre state, southwestern Amazonia: Fluvial or tidal? Deductions from the IGCP 449 fieldtrip. Journal of South American Earth Sciences, 21(1), 120–134.

Wood, L. J., 2007. Quantitative seismic geomorphology of Pliocene and Miocene fluvial systems in the northern Gulf of Mexico, USA. Journal of Sedimentary Research, 77, 713–730.

Zeng, H., 2007. Seismic imaging for seismic geomorphology beyond the seabed: potentials and challenges. Geological Society, London, Special Publications, 277, 15–28.

Zhuo, H., Wang, Y., Shi, H., He, M., Chen, W., Li, H., Wang, Y., Yan, W., 2015. Contrasting fluvial styles across the mid-Pleistocene climate transition in the northern shelf of the South China Sea: Evidence from 3D seismic data. Quaternary Science Reviews, 129, 128–146.

SUPPLEMENTARY DATA:

Name	Hor_slice_Amp.mpg
Caption/description	Animated seismic amplitude horizon slicing from surface (topography) to depth. The seismic amplitude horizon slices are displayed with a black (positive) to white (negative) scale bar.
Type	Video.
Format	MPG.
Duration	261 seconds.
Frame size	600x300 pixels.
Producer	Windows live movie maker and conversion from WMV to MPG file.

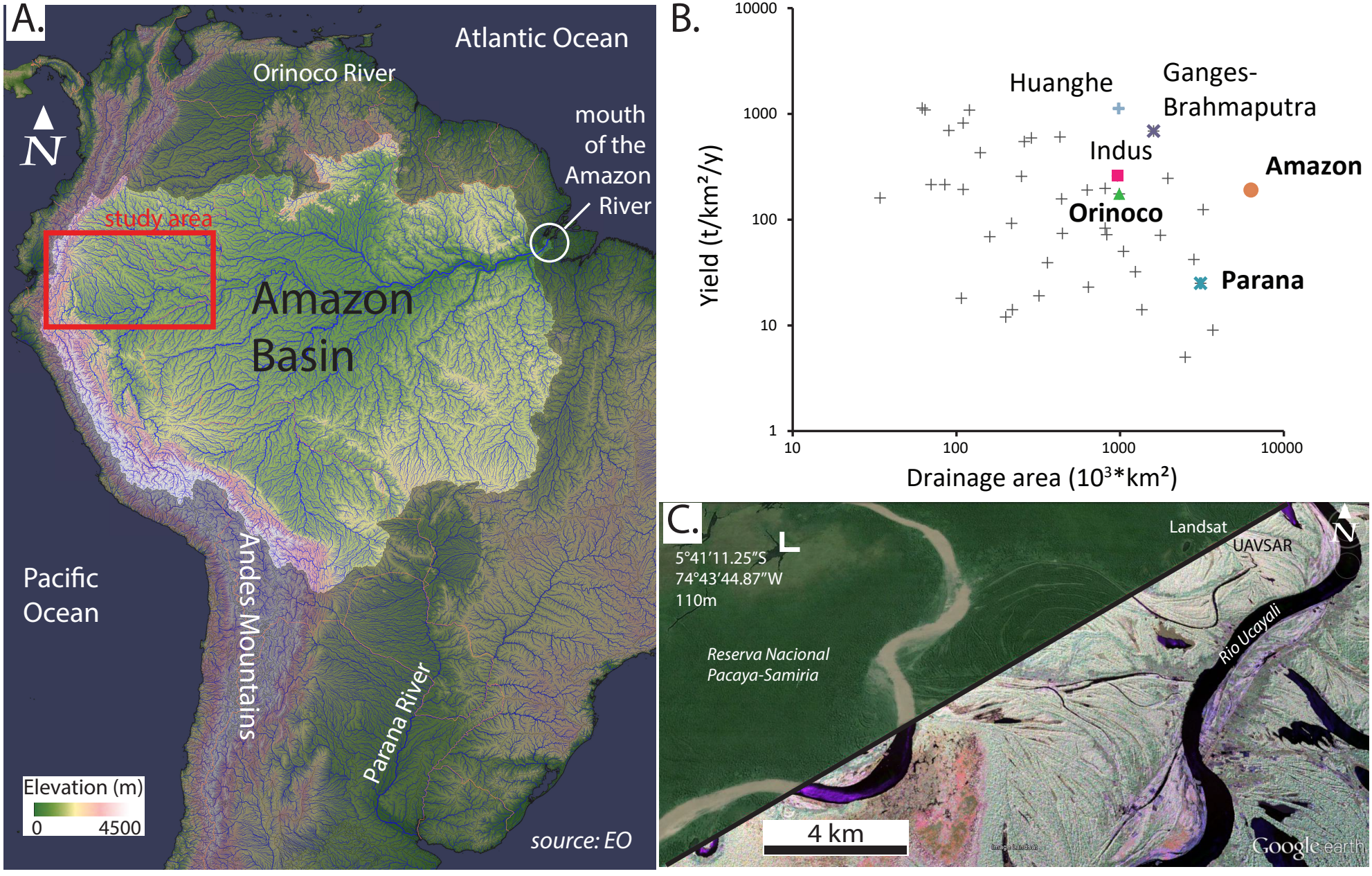
A.
Atlantic Ocean
Orinoco River
N
mouth of the Amazon River
study area
Amazon Basin
Pacific Ocean
Andes Mountains
Parana River
Elevation (m)
0
4500
source: EO
B.
Yield (t/km²/y)
Drainage area (10³*km²)
10000
1000
100
10
1
10
100
1000
10000
Huanghe
Ganges-Brahmaputra
Indus
Amazon
Orinoco
Parana
C.
5°41'11.25"S
74°43'44.87"W
110m
Reserva Nacional Pacaya-Samiria
Landsat
UAVSAR
N
Rio Ucayali
4 km
Google earth

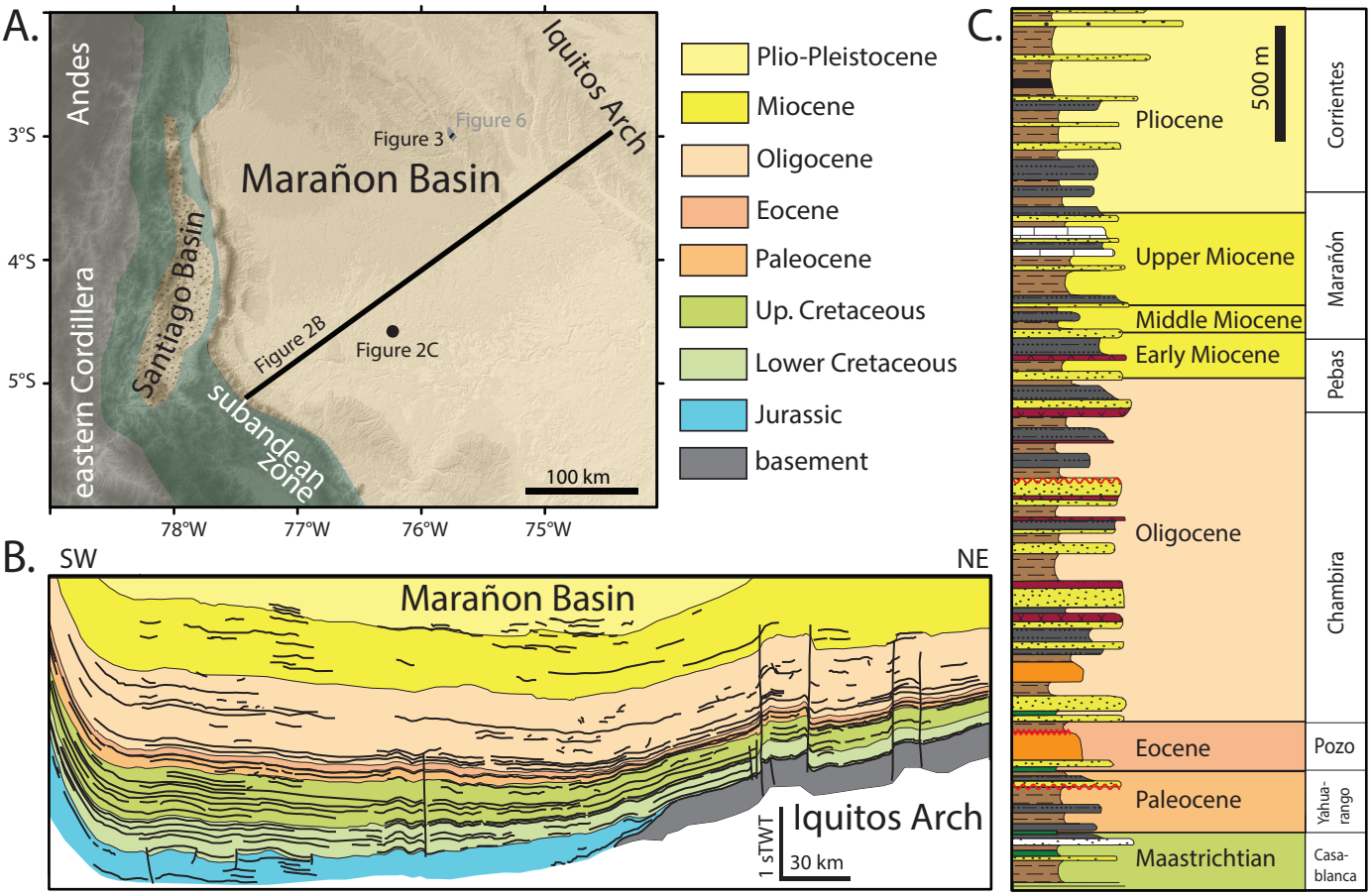
A.
Andes
eastern Cordillera
Santiago Basin
subandean zone
Marañon Basin
Iquitos Arch
Figure 3
Figure 6
Figure 2B
Figure 2C
100 km
3°S
4°S
5°S
78°W
77°W
76°W
75°W
Plio-Pleistocene
Miocene
Oligocene
Eocene
Paleocene
Up. Cretaceous
Lower Cretaceous
Jurassic
basement
B.
SW
NE
Marañon Basin
Iquitos Arch
1 sTWT
30 km
C.
500 m
Pliocene
Upper Miocene
Middle Miocene
Early Miocene
Oligocene
Eocene
Paleocene
Maastrichtian
Corrientes
Marañón
Pebas
Chambira
Pozo
Yahua-rango
Casa-blanca

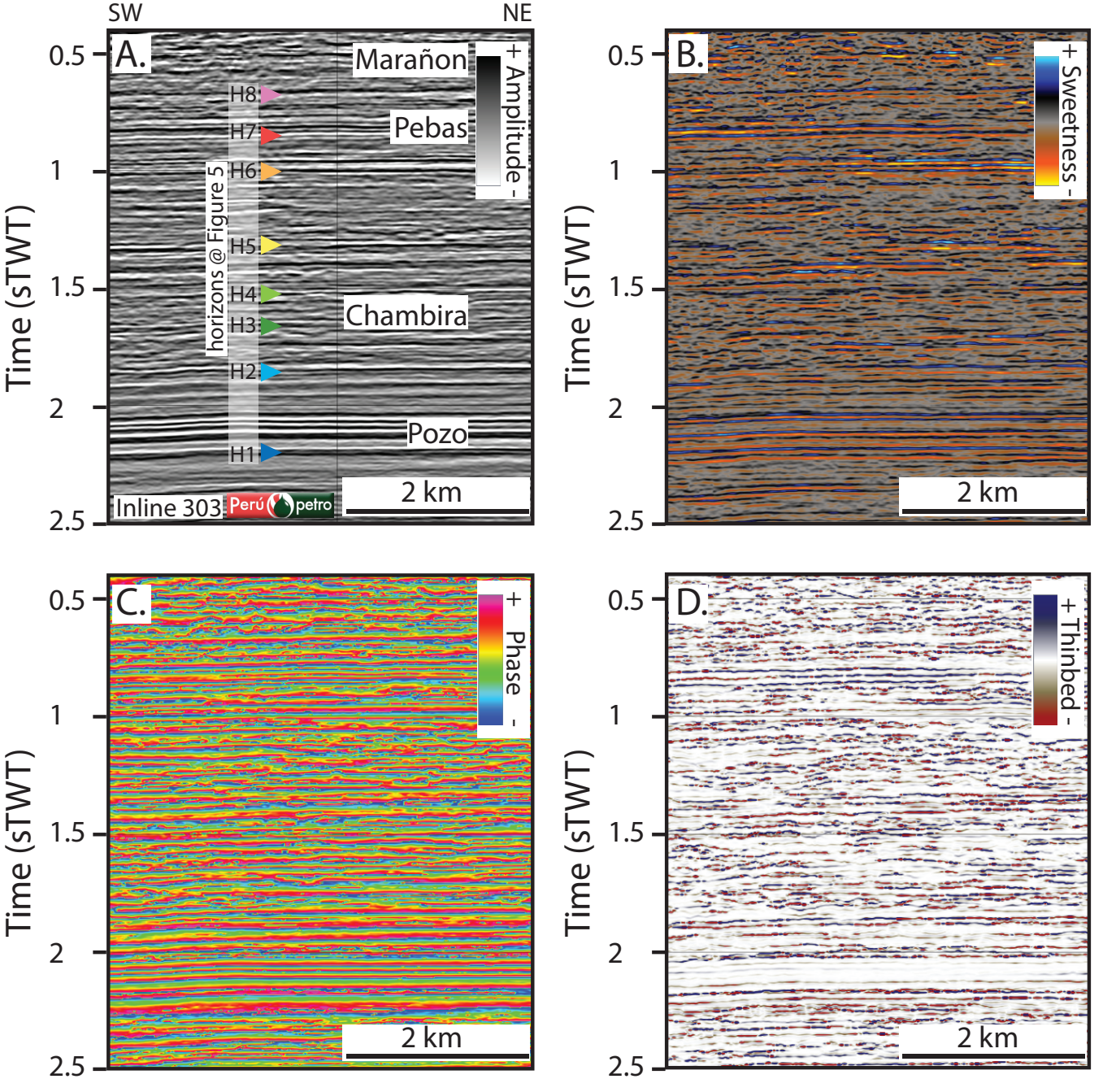
SW
NE
A.
Marañon
Pebas
Chambira
Pozo
H8
H7
H6
H5
H4
H3
H2
H1
horizons @ Figure 5
+ Amplitude -
Inline 303
Perú
petro
2 km
Time (sTWT)
0.5
1
1.5
2
2.5
B.
+ Sweetness -
C.
+ Phase -
D.
+ Thinbed -

Seismic facies	Seismic section + Amplitude -	Interpretation	Plan view + Amplitude -	Interpretation	Reflection character/Sedimentologic interpretation
SF1	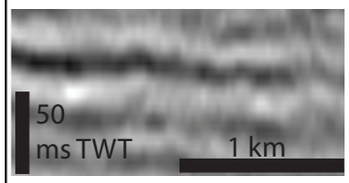	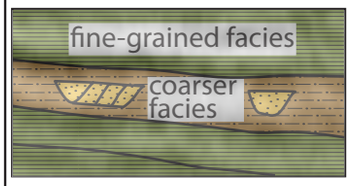	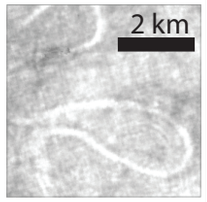	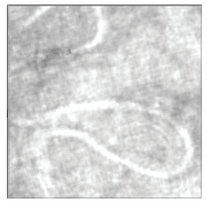	moderate to high amplitude, continuous reflection high amplitude related to channel peak frequency : 30 Hz channel width 100-200 m fluvial feature : meanders, high sinuosity and lateral accretion
SF2		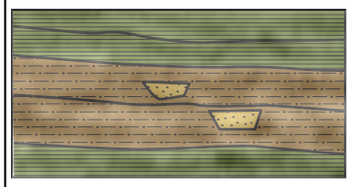	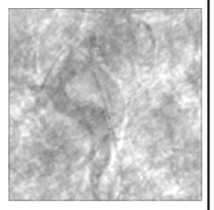	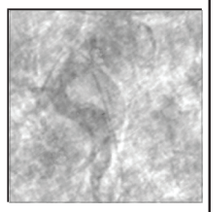	low to moderate amplitude, moderate continuity of reflection mixed amplitude change within larger channels peak frequency : 32 Hz channel width 70-650 m fluvial feature : meanders, moderate sinuosity and bars
SF3		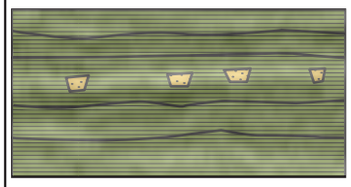	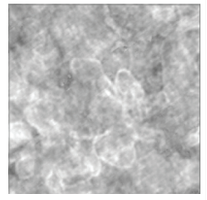	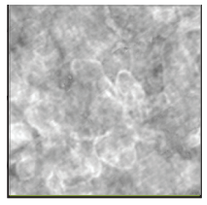	low to moderate amplitude, moderate continuity of reflection mixed amplitude change of channel eak frequency : 32 Hz channel width 70-270 m fluvial feature : meanders, moderate sinuosity and bars
SF4		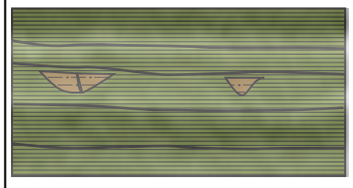	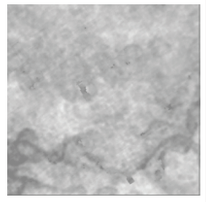	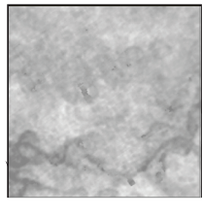	low amplitude, shingled to continuous reflection lowest amplitude related to channel peak frequency : 17 Hz channel width 80-300 m fluvial feature : meanders, low to moderate sinuosity
SF5		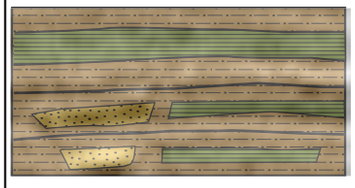	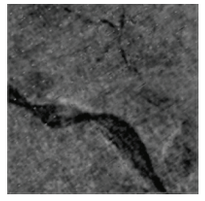	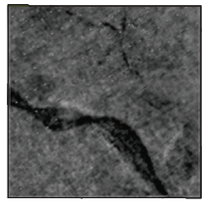	low to high amplitude, continuous reflection high amplitude related to channel peak frequency : 27 Hz channel width 80-300 m fluvial feature : meanders, low sinuosity and lateral accretion
SF6		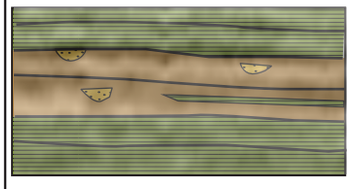	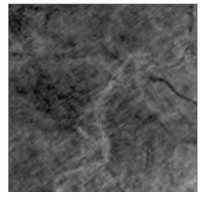	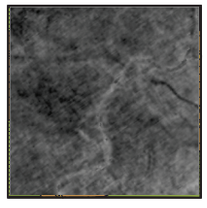	low to high amplitude, shingled to continuous reflection high amplitude related to channel peak frequency : 45 Hz channel width 40-360 m fluvial feature : meanders, low sinuosity, stacking and cross-cutting channels
SF7			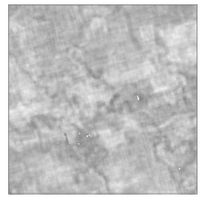	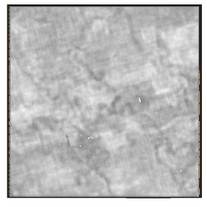	low to moderate amplitude, continuous reflection moderate amplitude related to channel peak frequency : 25 Hz channel width 100-150 m fluvial feature : anastomosing channel and cross-cutting channels
SF8	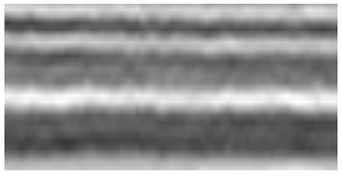	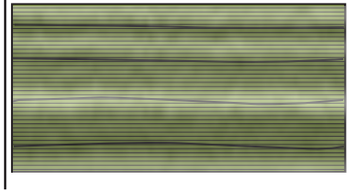		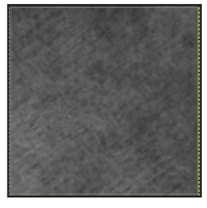	low to moderate amplitude, continuous reflection peak frequency : 22 Hz fluvial feature : flood plain?

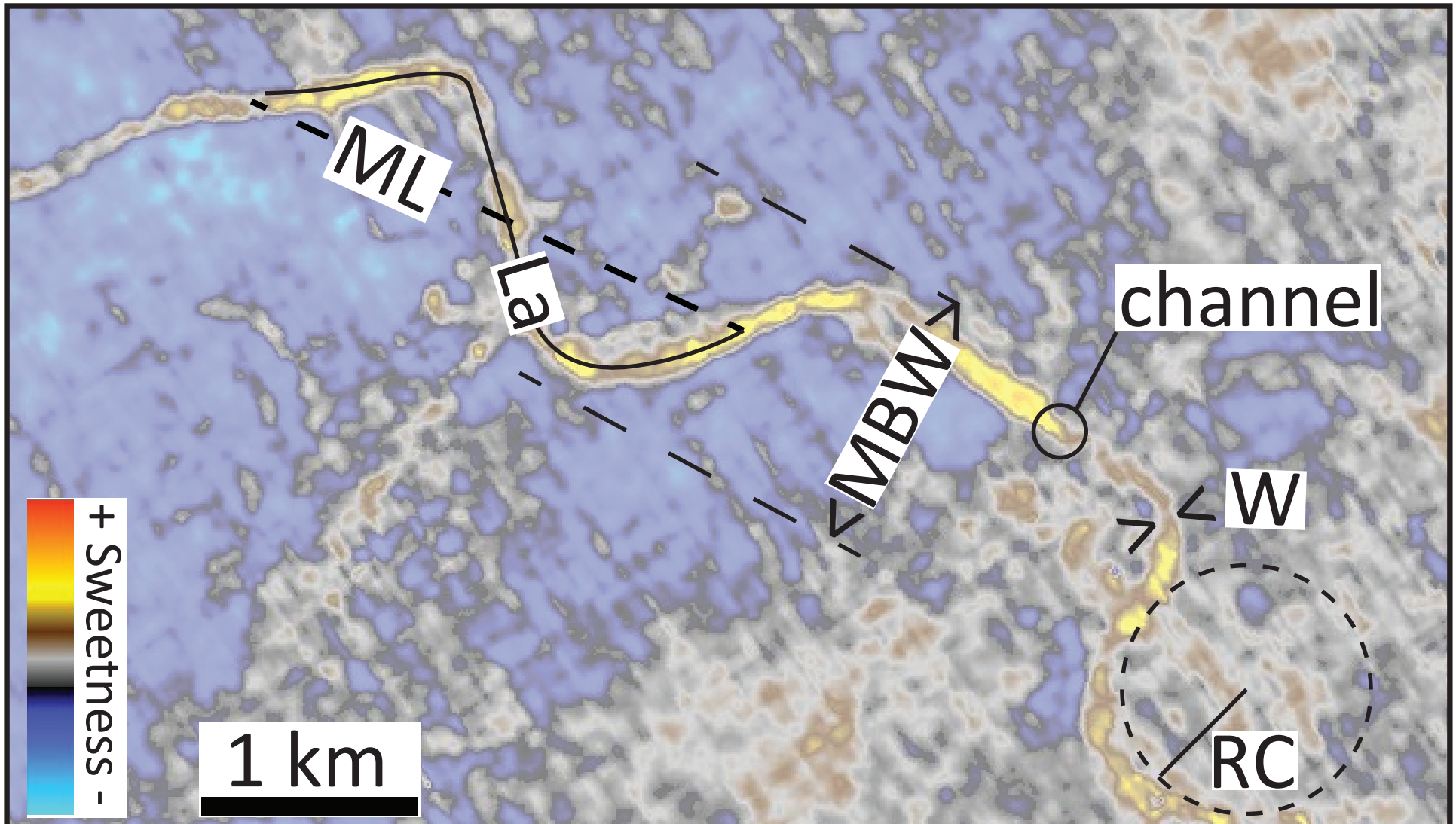
ML
La
MBW
channel
W
RC
1 km
+ Sweetness -

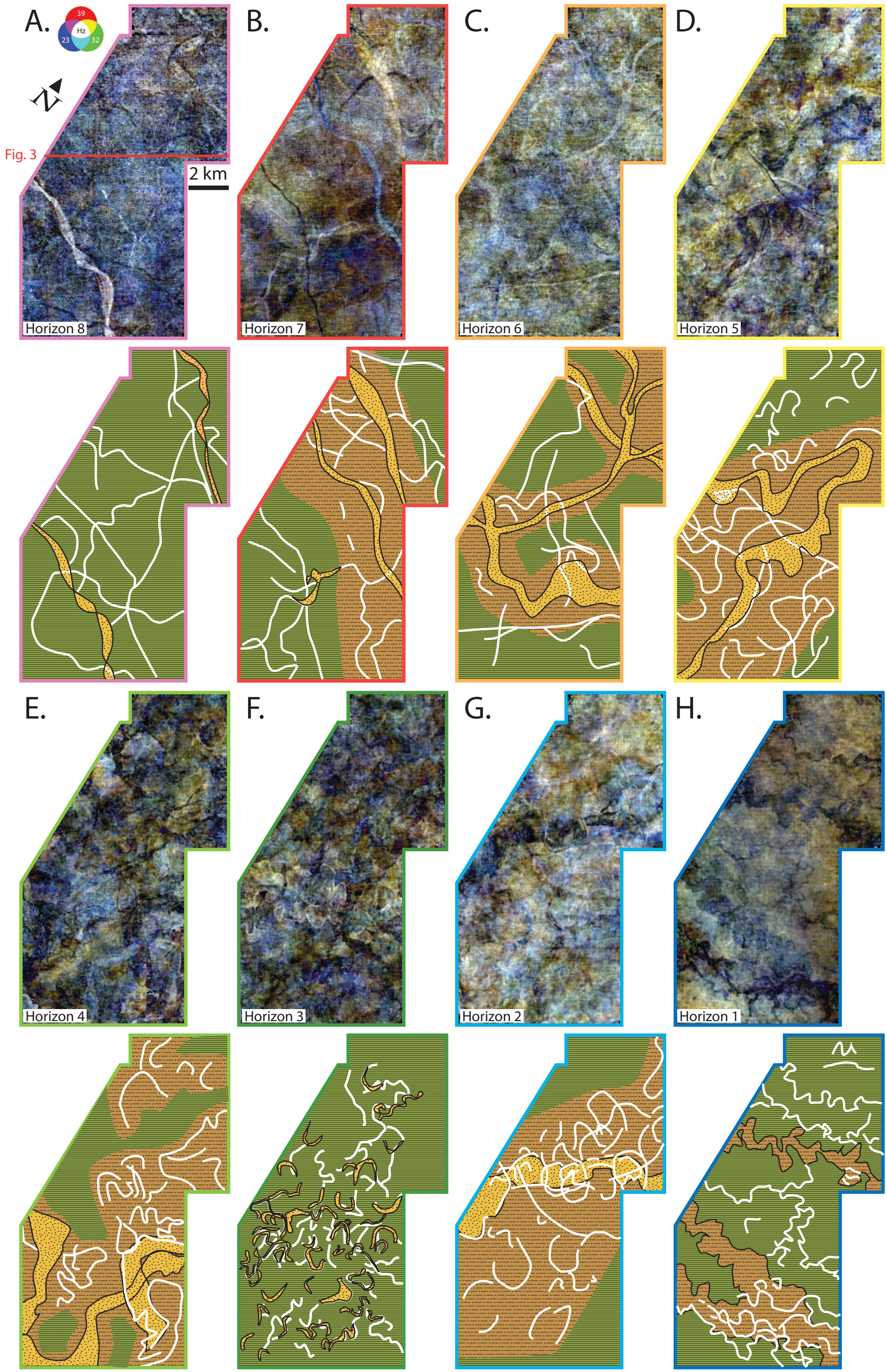
A.
39
Hz
23
32
N
Fig. 3
2 km
Horizon 8
B.
Horizon 7
C.
Horizon 6
D.
Horizon 5
E.
Horizon 4
F.
Horizon 3
G.
Horizon 2
H.
Horizon 1

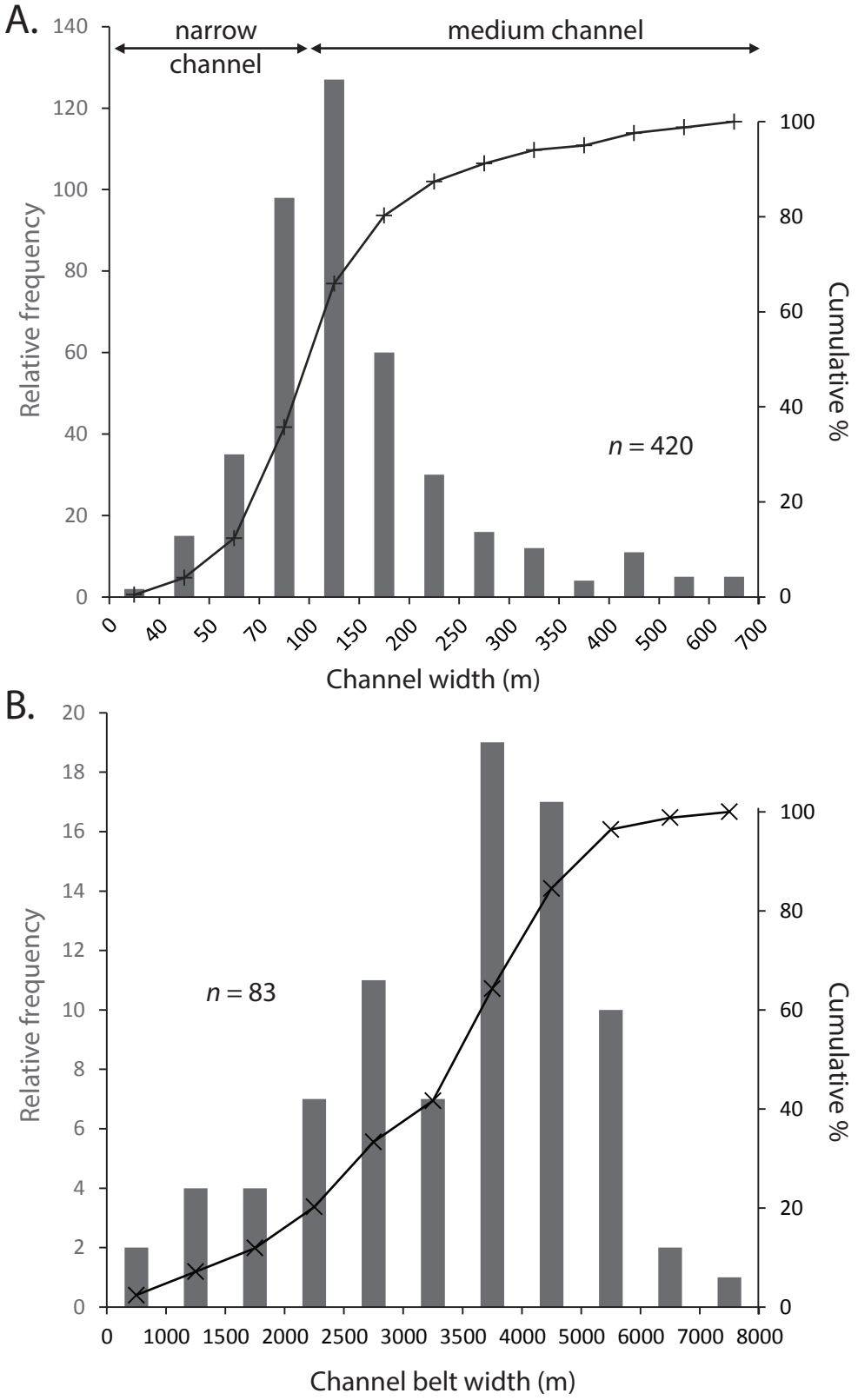
A.
narrow channel
medium channel
Relative frequency
Cumulative %
n = 420
Channel width (m)
0
40
50
70
100
150
200
250
300
350
400
500
600
700
B.
Relative frequency
Cumulative %
n = 83
Channel belt width (m)
0
1000
1500
2000
2500
3000
3500
4000
5000
6000
7000
8000

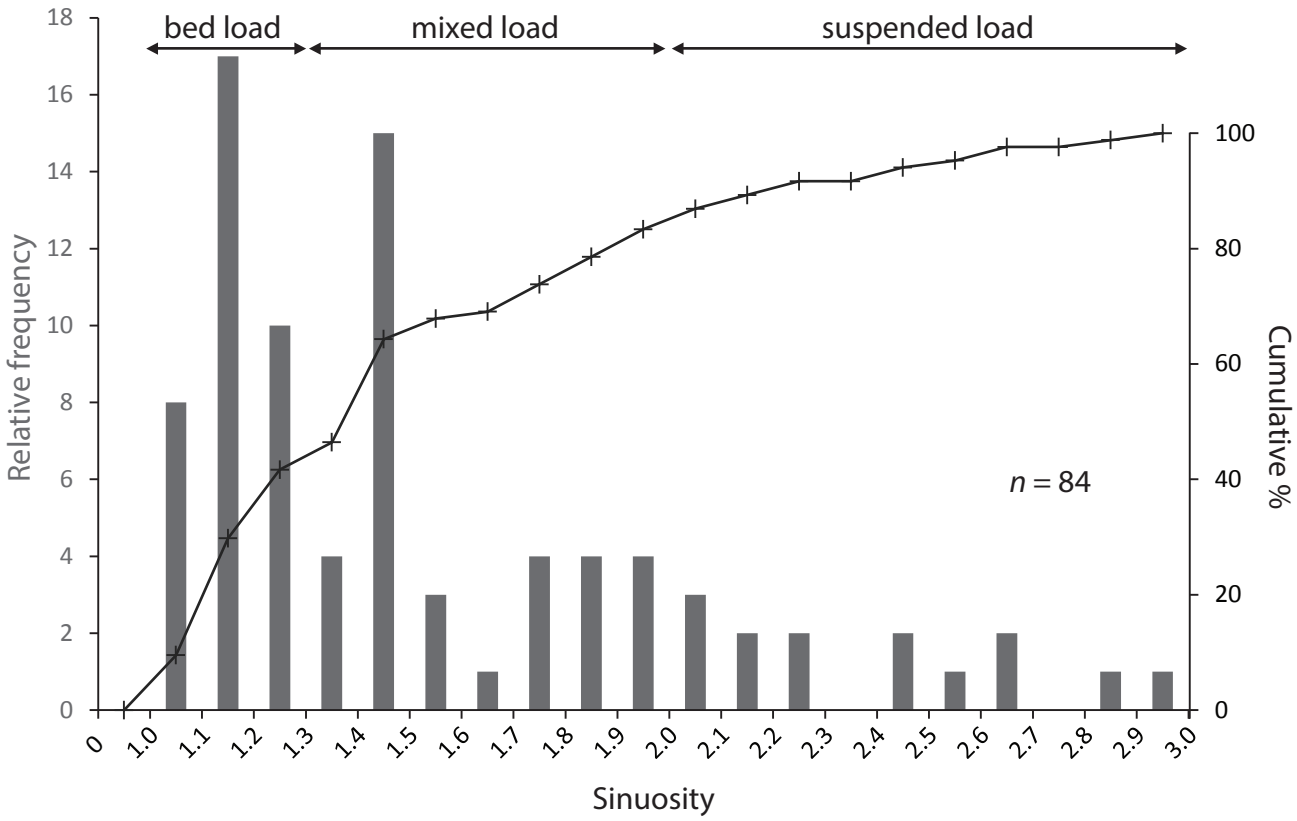
bed load
mixed load
suspended load
Relative frequency
Cumulative %
n = 84
Sinuosity
0
2
4
6
8
10
12
14
16
18
0
20
40
60
80
100
0
1.0
1.1
1.2
1.3
1.4
1.5
1.6
1.7
1.8
1.9
2.0
2.1
2.2
2.3
2.4
2.5
2.6
2.7
2.8
2.9
3.0

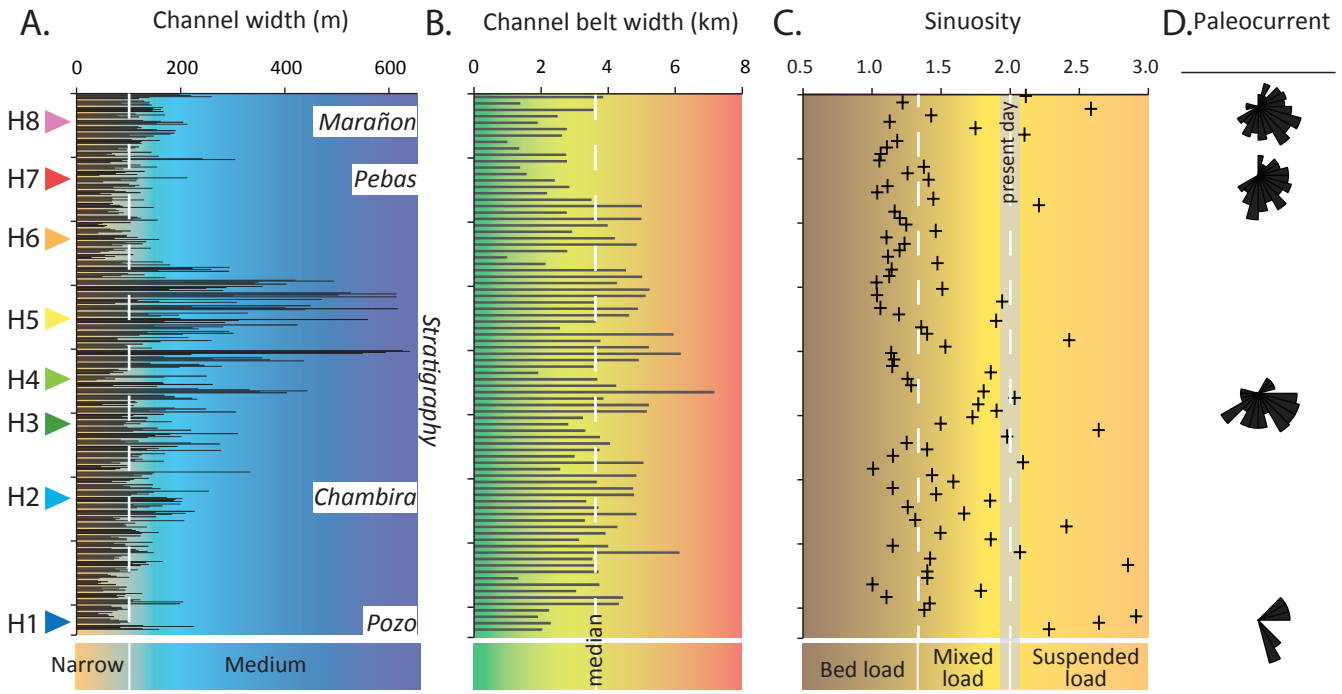
A.
Channel width (m)
0
200
400
600
H8
H7
H6
H5
H4
H3
H2
H1
Marañon
Pebas
Chambira
Pozo
Stratigraphy
Narrow
Medium
B.
Channel belt width (km)
0
2
4
6
8
median
C.
Sinuosity
0.5
1.0
1.5
2.0
2.5
3.0
present day
Bed load
Mixed load
Suspended load
D.
Paleocurrent

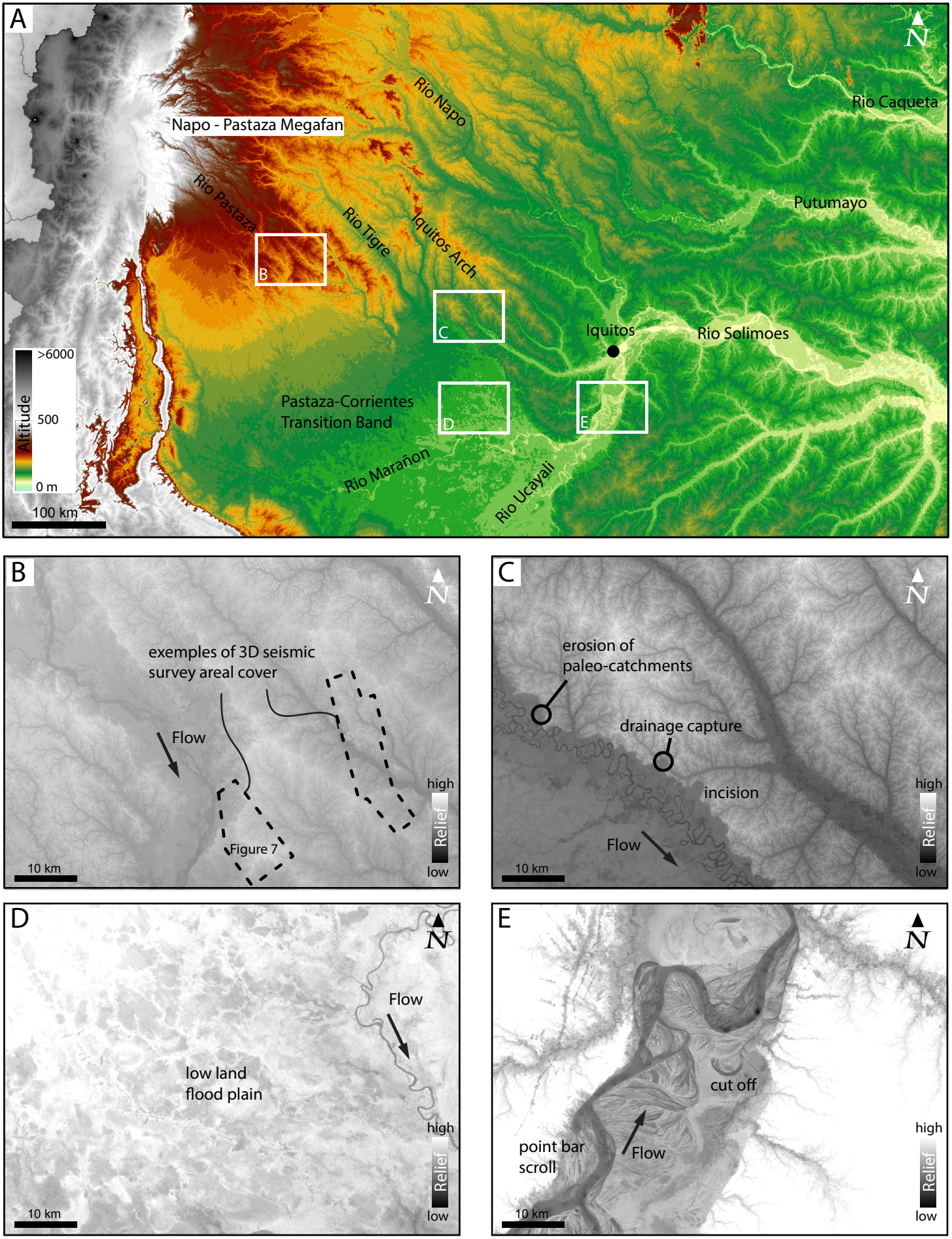
A
N
Napo - Pastaza Megafan
Rio Napo
Rio Caqueta
Rio Pastaza
Rio Tigre
Iquitos Arch
Putumayo
B
C
D
E
Iquitos
Rio Solimoes
>6000
Altitude
500
0 m
100 km
Pastaza-Corrientes
Transition Band
Rio Marañon
Rio Ucayali
B
N
exemples of 3D seismic
survey areal cover
Flow
Figure 7
high
Relief
low
10 km
C
N
erosion of
paleo-catchments
drainage capture
incision
Flow
high
Relief
low
10 km
D
N
Flow
low land
flood plain
high
Relief
low
10 km
E
N
cut off
point bar
scroll
Flow
high
Relief
low
10 km

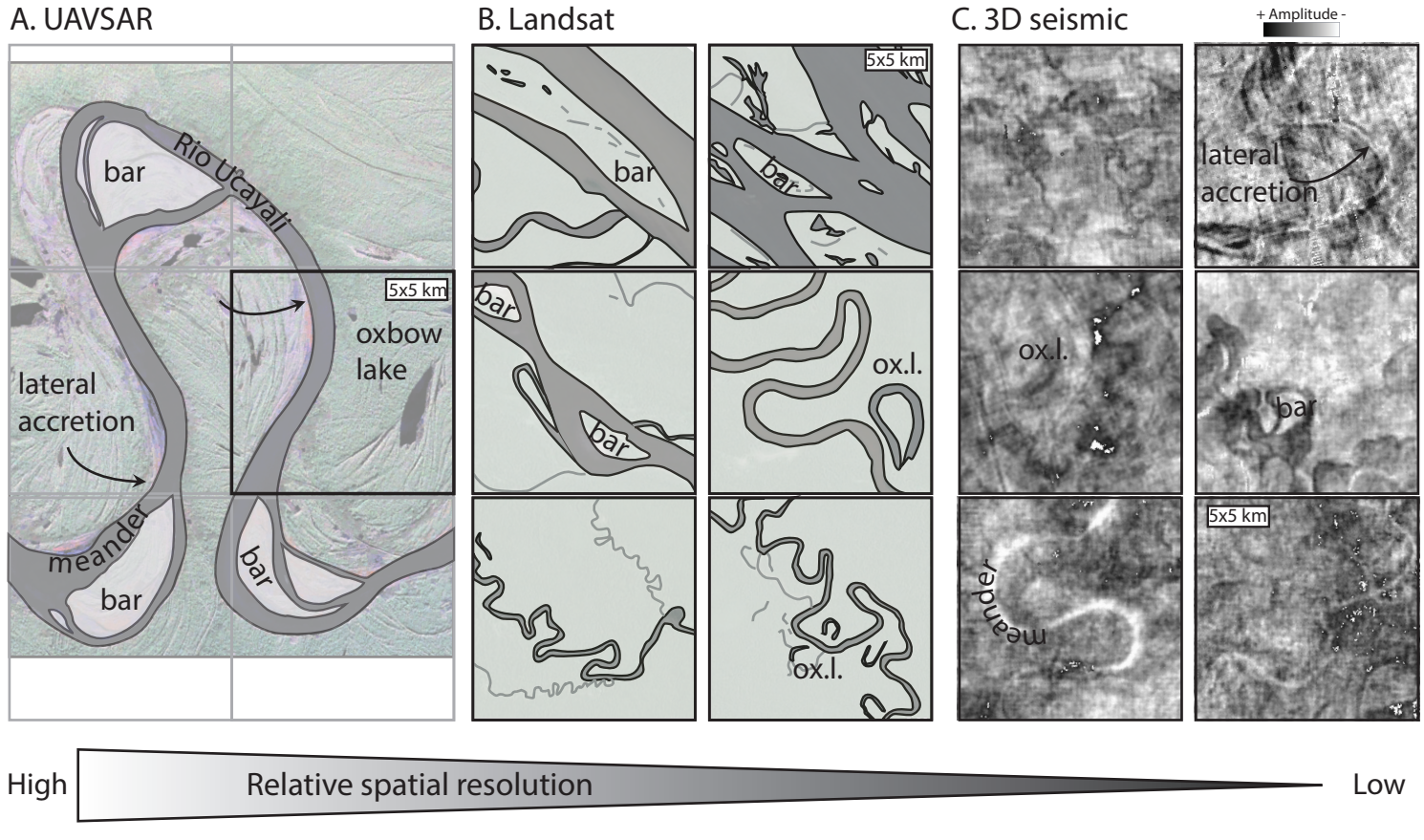
A. UAVSAR
B. Landsat
C. 3D seismic
+ Amplitude -
Rio Ucayali
bar
5x5 km
oxbow
lake
lateral
accretion
meander
bar
bar
bar
bar
bar
ox.l.
ox.l.
ox.l.
lateral
accretion
ox.l.
bar
meander
5x5 km
High
Relative spatial resolution
Low